Pak. j. sci. ind. res. Ser. A: phy. sci. 2022 **65A**(3) 248-259

Major Elements of Nari Formation Sandstone from Jungshahi Area of Southern Indus Basin, Pakistan

Asghar A.A.D. Hakro, Muhammad Soomar Samtio, Riaz Hussain Rajper* and Abdul Shakoor Mastoi

Centre of Pure and Applied Geology, University of Sindh, Jamshoro-76080, Pakistan

(received October 10, 2019; revised July 14, 2021; accepted July 27, 2021)

Abstract. This study is carried out for geochemical investigation of the Nari formation from Jungshahi area southern Indus basin, Pakistan. Six rock samples of Nari formation were analyzed for the information of classification, paleo-weathering conditions, provenance and tectonic setting of Oligocene (33.9-23.03 Ma) geological time. The study of major elements (Si, Ti, Al, Na, Ca, K, Mn, Mg, Fe^{+3}, P and S) and their ratios indicate that the Nari formation is dominantly composed of intermediate quartz. The silica has originated as either bio-genically precipitated or in detrital modes. Most of the sediments are detritus from the study area and Oligocene formation is composed of sandstone with subordinate shale. Field observation reveals that most of the sandstone is consolidated, calcareous and ferruginous. This sandstone is variegated in colour, light grey to dark grey, camel and red in colour at some places. The geochemical classification of Nari sandstone classified as the Subarkose and sub-litharenite and quartz-arenite. The CIA, PIA and CIW values indicate that, the Nari formation is deposited under low weathering conditions in the southern Indus basin during Oligocene time in an arid climate. Major elements indicate the sediments of Nari formation were supplied from the Mafic to Intermediate igneous source. The provenance and tectonic setting demonstrate that oligocence sediments of Nari formation sediments were deposited in tectonically in an active continental margin.

Keywords: Nari formation, Oligocene, Jungshahi area, southern Indus basin, tectonic setting

Introduction

Geochemistry provide insight into the broader composition of the rock types and they help to determine provenance, weathering, tectonic setting and diagenesis (Hakro *et al*., 2021; Samtio *et al*., 2021; Hakro *et al*., 2015; Bhatia and Crook, 1986; Bhatia, 1983). Studies on the composition of sedimentary rocks have significantly improved our understanding of the tectonic history of the earth (Kassi *et al*., 2009; Taylor and McLennan, 1985; Dickinson and Valloni, 1980). The provenance and nature of weathering are important geochemical signs of clastic sediments for the information of the source of clastic sediments (Kettanah *et al*., 2021; Hao *et al*., 2018; Yan *et al*., 2007). The major elemental geochemistry are particularly helpful in the identifying the signatures of source, topography, denudation and tectonic history of the area of sedimentary rock (Blanco *et al*., 2021; Maravelis *et al*., 2021; Roser and Korsch, 1988). The process of denudation, diagenesis and lithification seems to be responsible for the geochemical composition of the clastic sediments (Li *et al*., 2021; Hakro and Khokhar, 2015). Major elements (Si, Ti, Al, Na, Ca, K, Mn, Mg, Fe^{+3}, S and P) of Nari formation are studied to determine the chemical properties and the tectonic setting, provenance, Paleo-weathering of the Nari formation from Jungshahi area, Sindh, province, Pakistan shown in (Fig. 1a and 1b). The composition of provenance probably has major control on the chemistry of sedimentary rocks although this can be greatly modified by weathering, transportation, deposition and diagenesis processes. In this regard, the rock samples of Nari formation were used for geochemical studies. Previously southern Indus basin was considered as foreland basin since decades, related to the India and Asia collision and timing of collision remains matter of debate (Hakro *et al*., 2021 and 2018). However, due to the lack of systematic data of provenance and tectonic setting the geodynamic link of SIB is missing with reference to India and Asia collision. The key objective of this paper is to identify the provenance and tectonic setting of Oligocene epoch and to recommend major element geochemical criteria to differentiate plate tectonic settings of of southern Indus basin.

Geologically studied area is located in the Southern Indus Basin (SIB), which is the part of (lower Indus

*Author for correspondence;
E-mail: riazgeophysicist@usindh.edu.pk

basin). Tertiary rocks are well exposed in SIB, Pakistan (Hakro and Khokhar, 2015). The study area is located at Jungshahi, Thatta on Toposheet No: 35 P/13 and geologically it lies in SIB, Pakistan having (Lat: 24° 38′ 08″ N and Long: 67° 22′ 21″ E). Chronological order Nari formation is placed into the Oligocene epoch of geological time scale of Sindh (Hakro *et al*., 2021; Shah, 2009). The upper part of the Nari formation predominantly composed of sandstone, which is greenish grey, grey-brown and white in colour and texturally it is fine to coarse-grained often gritty and calcareous with subordinate shale, sandstone and variegated colour of claystone (Shah, 2009). Nari formation has been investigated on petrographical studies by various scholars (Samtio *et al*., 2021; Shar, 2021; Khokhar *et al*., 2016; Agheem *et al*., 2012; Shah, 2009; Mahmud and Sheikh, 2009; Duncan and Sladen, 1884; Farshori, 1972; Iqbal, 1969; Khan, 1968). We have done work in the light of geochemistry, Lithological log of Jungshahi area (Fig 2.), which represents the different facies thickness of Nari formation.

Materials and Methods

The stratigraphic section of Nari formation was measured for true thickness with Jacob's staff method, through the bed to bed because the position of beds was low dipping and almost were in a horizontal form. The total thickness of Nari formation is 24 meters thick, where we have collected 13 samples. Six representative samples

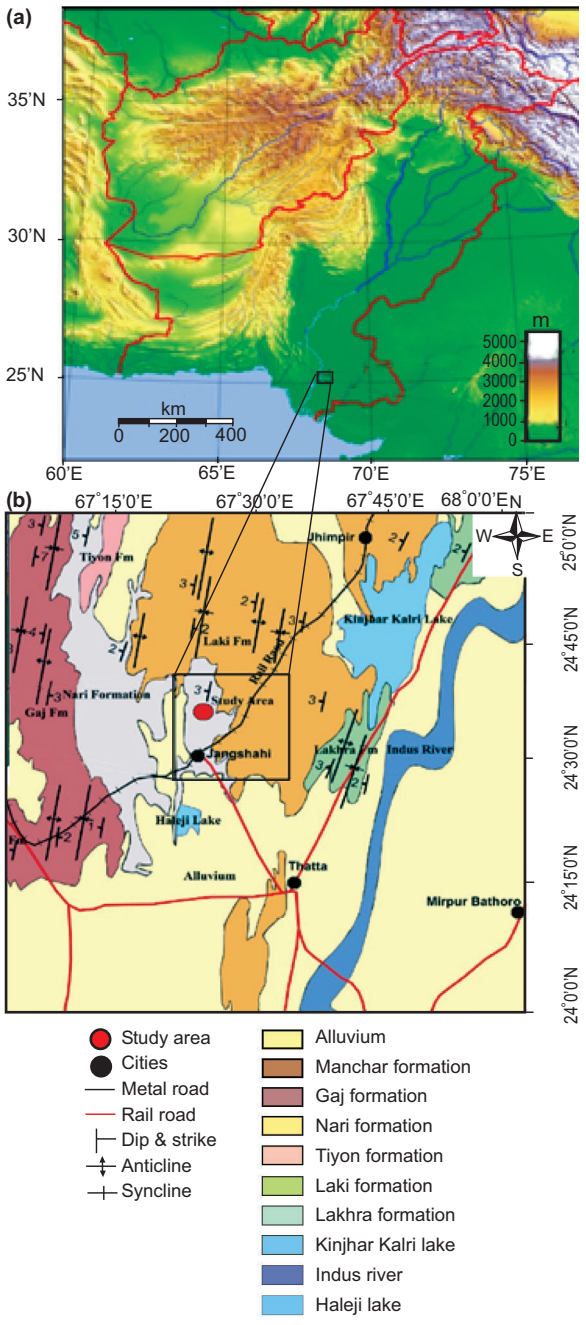

Fig. 1. **(a)** and **(b)** shows the location map of study area modified (after Geological Survey of Pakistan (GSP) 2012 (HSC, 1961).

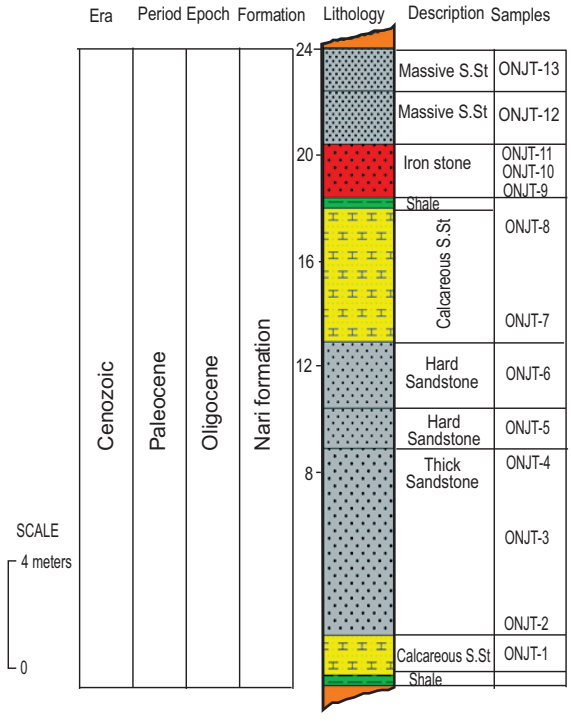

Fig. 2. Shows columnar section of the study area, lithological column of the Nari formation from Jangshahi, Thatta.

of sandstones have selected for major elemental composition. The pellets of the rock samples were prepared as raw rock samples and were analyzed by X-ray fluorescence model S4-PIONEER equipped at Centre for Pure and Applied Geology, University of Sindh, Jamshoro. All samples were run on X-ray fluorescence (XRF) model S4-PIONEER for investigation of major element analysis. The preparation of samples and procedure were adopted according to (Glocker and Schreiber, 1928).

Six samples out of thirteen samples were selected for XRF, the rock samples were crushed into small chips and chips were loaded into the grinding mill and pulverized for 20 min, then for 3 min samples were grinded in a grinding mill to obtain 200 mesh sizes. For each rock sample the grinding machine was cleaned and washed with the distilled water to avoid the contamination of previous rock powder. The pellets were prepared from 10 g of 200 mesh size powdered of rock sample then put 3 g of binder (2% aqueous solution of polyvinyl pyrolidine) were added and mixed with the pestle manually. This paste was put into cylinder and pulled out gently and finely powdered boric acid was added to paste. A stainless steel plunger was inserted and the paste was pressed at about 25N (neutons) for nearly 3 min, in a hydraulic pressure. The pressure was released slowly and gradually the finally the pellet was ready to run further process. After making the pellets these were kept with the sample bags and placed the numbering with the permanent marker. After making pellets these rock samples were run in the XRF machine model no (S-4 PIONEER) available at the advance Research Laboratory of Centre for Pure and Applied Geology, University of Sindh, Jamshoro, Pakistan.

The six samples out of 13 were analyzed for major elements concentration including Si, Ti, Al, Fe* (total iron) Mg, Ca, Na, K, S and P oxides in weight. The samples are labeled as JT-1, JT-3, JT-6, JT-7, JT-8, JT-9 for Nari formation from Jungshahi area.

Results and Discussion

Major elements. The concentrations of major elements and correlation coefficient values from six representative sandstone samples are present in the Table 1 and 2 along with selected pairs of major elements. The ratio silicon dioxide (SiO_2) from studied samples vary from 51.5-68.3 wt. % with average ~58.08 wt. % maximum concentration is reported in sample JT-09 (68.3 wt.%). The concentration ratio of Al_2O_3 varies from 0.47-7.24 wt. % with an average of 4.79 wt. % maximum concentration is reported in sample JT-09 7.24 wt. % of Al_2O_3. The ratio of Titanium dioxide (TiO_2) varies from 0.08-0.43 wt. % with an average of 0.31 wt. % TiO_2 maximum concentration is reported in sample JT-010.43 wt. %, TiO_2 and Fe_2O_3 varies from 4.17-18.98 wt.% with an average of 11.22 wt. %, the maximum concentration of ironoxide (Fe_2O_3) is observed from sample JT-09 with average ~18.98 wt. %, Magnesium oxide (Fe_2O_3). MgO varies from 0.1-6.5 wt. % with an average of 3.04 wt. %, MgO maximum concentration is marked in sample JT-06 (6.5 wt. %), while sodium dioxide (NaO_2) varies from 0.15-0.98 wt. % with an average of 0.45 wt. % maximum concentration is reported in sample JT-09 (0.98 wt. %) and Calcium oxide (CaO) varies from 0.81-28.8 wt. % CaO with average ~17.47 wt. % maximum concentration is reported in sample JT-06 (28.8 wt. %). Magnese oxide (MnO) varies from 0.05-0.40 wt. % with an average of 0.23 wt. % maximum concentration is reported in sample JT-06 (0.4 wt. %). Potassium oxide (K_2O) varies from 0.03-1.15 wt. %, with average ~0.84 wt. % maximum concentration is reported in sample JT-03 (1.15 wt %). Phosphorus oxide (P_2O_5) varies from 0.06-0.22 wt. % P_2O_5 with an average of 0.11 wt. % maximum con-centration is reported in sample JT-01 (1.15 wt. %) of P_2O_5.

Harker's bivariate diagram is used for Nari formation sandstone of Jungshahi area. Harker diagrams are presented to compare the abundances of major element oxides along a common axis namely SiO_2 (Fig. 3).

In (Fig. 3d) SiO_2 shows a weak positive correlation with Al_2O_3 with 0.206 correlation coefficient values which indicate that both elements were supplied from the same source. In (Fig. 3b) SiO_2 shows a negative correlation with TiO_2 with -0.334 correlation coefficient values which indicates that these both elements were supplied from the same source. In (Fig. 3a) SiO_2 shows a moderately positive correlation of Fe_2O_3 with 0.419 correlation coefficient values which indicates that these elements were supplied from the same source. In (Fig. 3h) SiO_2 shows a negative correlation of MgO with -0.662 correlation coefficient value which indicates that these elements were not supplied from the same source. In (Fig. 3c) silicon dioxide (SiO_2) shows a positive correlation with NaO_2 (0.609) correlation coefficient value which indicates that these both elements were not supplied from the same source, while in (Fig. 3e) SiO_2 shows a negative correlation with CaO with -0.665 correlation coefficient value which indicates

that these both elements were not supplied from the same source and in (Fig. 3f) SiO_2 shows a negative correlation with MnO with -0.712 correlation coefficient value which indicates that these both elements were supplied from the same source. In (Fig. 3g) SiO_2 shows a insignificant correlation with K_2O with 0.094 correlation coefficient value which indicates that these both elements were not supplied from the same source. In (Fig. 3i) SiO_2 shows a weak positive correlation with P_2O_5 with 0.218 correlation coefficient value which indicates that these both elements were not supplied from the same source.

Table 1. Major elements concentration in (weight %) and different ratios calculated from major oxides

Major elements	JT-1	JT-3	JT-6	JT-7	JT-8	JT-9	Average
SiO_2%	60.1	57.1	51.5	56.1	55.4	68.3	58.08
Al_2O_3%	0.47	5.47	4.51	4.92	6.11	7.24	4.79
TiO_2%	0.43	0.4	0.14	0.36	0.42	0.08	0.31
Fe_2O_3%	9.57	5.36	4.76	4.17	24.5	18.98	11.22
MgO%	0.1	5.6	6.5	5.31	0.52	0.2	3.04
NaO_2%	0.2	0.76	0.43	0.15	0.17	0.98	0.45
CaO%	23	21.6	28.8	25.5	5.11	0.81	17.47
MnO%	0.35	0.15	0.4	0.2	0.25	0.05	0.23
K_2O%	0.03	1.15	0.37	1.08	1.34	1.04	0.84
P_2O_5%	0.22	0.06	0.06	0.07	0.17	0.1	0.11
SO_3%	0.32	0.13	0.45	0.15	0.41	0.12	0.26
LOI	4.413	1.738	1.734	1.685	5.472	1.495	2.76
Total	99.227	99.528	99.674	99.7122	99.91	99.4356	99.58
SiO_2/Al_2O_3	127.872	10.438	11.419	11.402	9.067	9.423	29.94
Al_2O_3/SiO_2	0.007	0.095	0.087	0.087	0.11	0.106	0.08
Al_2O_3/NaO_2	2.35	7.197	10.488	32.8	34.519	7.365	15.79
K_2O/Al_2O_3	0.076	0.21	0.083	0.219	0.219	0.143	0.16
TiO_2/Al_2O_3	0.914	0.073	0.031	0.073	0.069	0.011	0.20
Fe_2O_3/Al_2O_3	20.361	0.979	1.055	0.847	4.009	2.618	4.98
NaO_2/K_2O	5.555	0.66	1.14	0.138	0.132	0.944	1.43
MnO/Fe_2O_3	0.037	0.029	0.084	0.049	0.01	0.003	0.04
MgO/Al_2O_3	0.212	1.023	1.441	1.079	0.086	0.027	0.64
CIA	1.98	18.88	13.22	15.55	48.00	71.90	
PIA	1.86	16.19	12.41	13.02	47.46	77.60	
CIW	1.99	19.66	13.37	16.09	53.64	80.18	

Table 2. Shows the correlation coefficient values

Major oxides	SiO_2%	Al_2O_3%	TiO_2%	Fe_2O_3%	MgO%	NaO_2%	CaO%	MnO%	K_2O%	P_2O_5%	SO_3%
SiO_2%	1	-	-	-	-	-	-	-	-	-	-
Al_2O_3%	0.206	1	-	-	-	-	-	-	-	-	-
TiO_2%	-0.334	-0.459	1	-	-	-	-	-	-	-	-
Fe_2O_3%	0.419	0.409	-0.046	1	-	-	-	-	-	-	-
MgO%	-0.662	0.098	-0.094	-0.796	1	-	-	-	-	-	-
NaO_2%	0.609	0.540	-0.619	0.083	-0.004	1	-	-	-	-	-
CaO%	-0.665	-0.597	0.222	-0.923	0.735	-0.401	1	-	-	-	-
MnO%	-0.712	-0.693	0.206	-0.317	0.215	-0.667	0.638	1	-	-	-
K_2O%	0.094	0.842	0.079	0.412	0.034	0.225	-0.541	-0.708	1	-	-
P_2O_5%	0.218	-0.574	0.470	0.503	-0.820	-0.820	-0.274	0.297	-0.365	1	-
SO_3%	-0.614	-0.324	0.057	0.176	-0.036	-0.548	0.179	0.847	-0.412	0.369	1

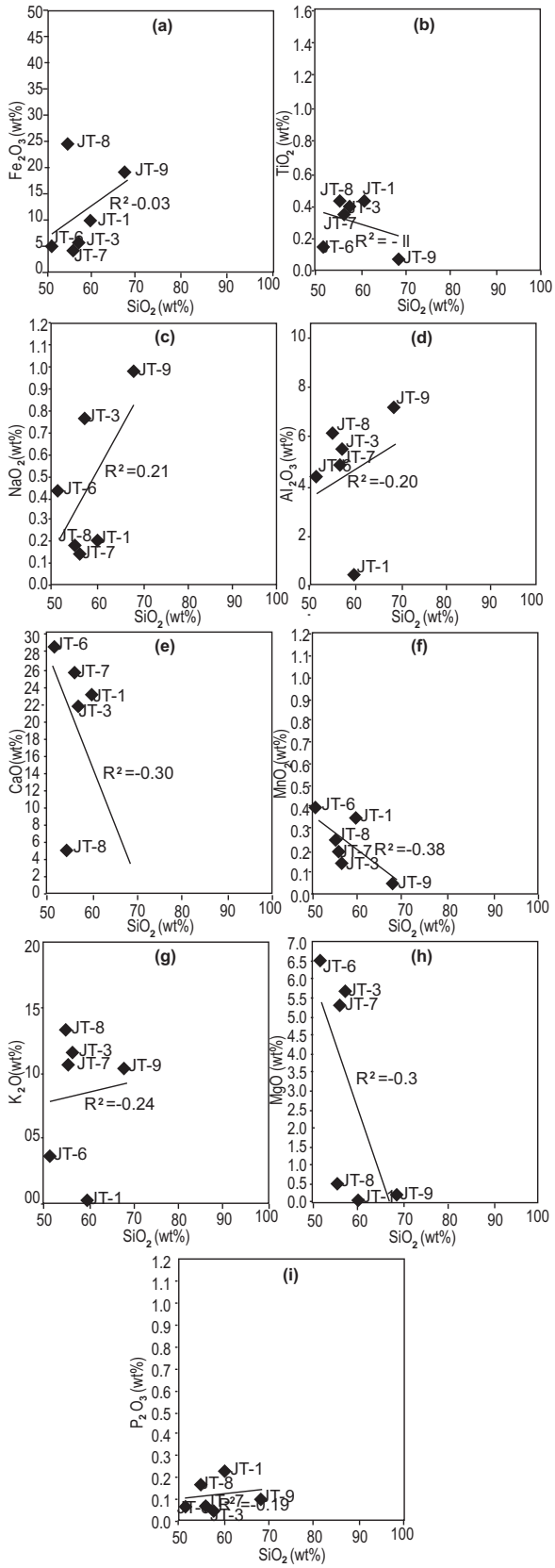

Fig. 3. Harker's bivariate diagram of Nari formation from Jungshahi, southern Indus Basin, Pakistan.

Geochemical classification of sandstone from Nari formation. On the bais of chemical composition Sandstones are classified as presented by (Herron, 1988; Crook, 1974; Pettijohn *et al*., 1972). Sandstone of Nari formation was classified according to the scheme proposed by (Pettijohn *et al*., 1972). The bivariate diagram in which log (SiO_2/Al_2O_3) along the X-axis versus log (NaO_2/K_2O) along the Y-axis. In this diagram, six different fields are presented as Greywacke, Litharenite, Subarkose, Arkose, Sub-litharenite and Quartzarenite. Three sandstone samples of Nari formation (JT-3, 6, 9) were plotted in the field of Subarkose, two sandstone samples (JT-7, 8) were plotted in Sublitharenite field and remaining one sample (JT-1) is plotted in the field of Quartzarenite (Fig. 4a).

The sandstone of Nari formation was classified as suggested by (Herron, 1988). In the bivariate log (Fe_2O_3/K_2O) along the Y-axis versus log (SiO_2/Al_2O_3) along the X-axis diagram (Herron, 1988) and this diagram is divided into nine fields namely Fe-shale, Fe-sand, Quartzarenite, Shale, Wacke, Litharenite, Sublitharenite, Subarkose, Arkose and Subarkose. Out of 6 samples 5 samples from Nari formation, (JT-3, 6, 7, 8 and 9) were plotted in the field of Fe-sand and one sample (JT-1) is plotted in the Quartzarenite field (Fig. 4b).

According to Crook (1974) sandstone is classified into 3 types (quartz-rich, quartz intermediate and quartz-poor) based on their Na_2O and K_2O contents. Five sandstone samples of Nari formation (JT-3,6,7,8 and 9) are mostly plotted in quartz-rich and quartz intermediate and from them, one sample (JT-1) plotted in poor quartz (Fig. 4c). However, the sandstone of present work has a lower concentration of SiO_2 (average SiO_2 content: 58.08 wt. %) in comparison with typical quartz rich sandstones (average SiO_2 content: 89 wt. %).

Weathering of the source area. The geochemical amalgamation of sediments almost depends on the source rocks and basically, these sediments are influenced by denudation, storage, deposition and diagenesis. Therefore, geochemical characters can notify the conditions of sediments information processes (Hakro *et al*., 2021 and 2018; Shar, 2021) weathering indices of sedimentary rocks can supply useful information about tectonic activity and climatic conditions in the source region. The increase of degree in chemical weathering may reflect the decrease in tectonic activity and change of climate towards warm

and humid conditions which are more favourable for chemical weathering in source region (Jacobson and Blum, 2003). In general terms, alkali and alkaline earth elements offer information for weathering sources (Nesbitt and Young, 1996). The Chemical Index of Alteration (CIA), Plagioclase Index of Alteration (PIA), and Chemical Index of Weathering (CIW) scheme of (Nesbitt and Young, 1982) are widely used to measure source area. The CIA, PIA and CIW values of sandstone from Nari formation varies from 1.9 to 71.84 wt. % with an average ~28.22, 1.83 to 77.51 wt. % with an average of 28.06 wt. % and 1.98 to 80.10 wt. % with

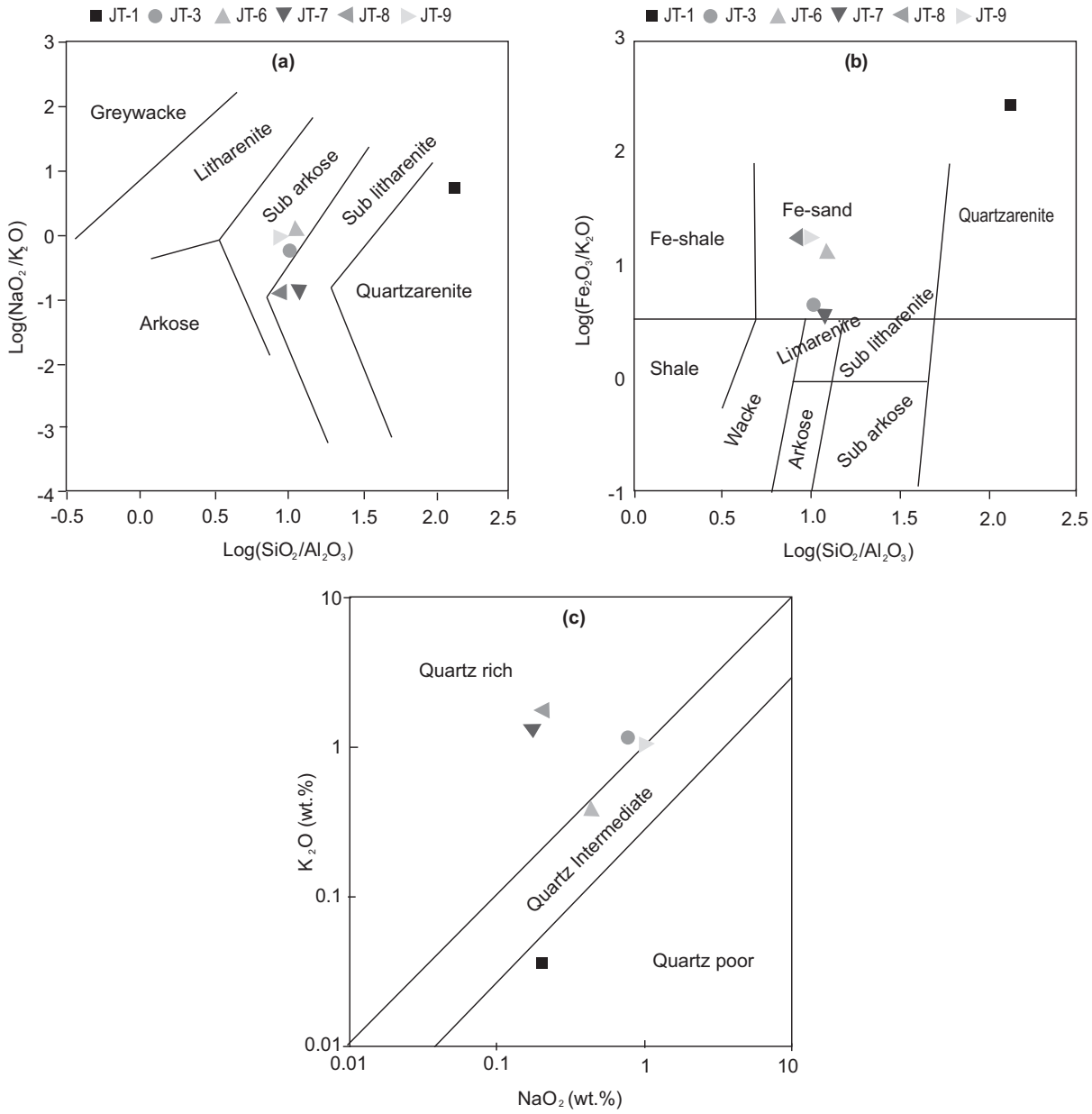

Fig. 4. **(a)** Geochemical classification diagram discriminating sediments according to logarithmic ratios of SiO_2/Al_2O_3 versus NaO_2/K_2O after (Pettijohn *et al*., 1972), **(b)** Geochemical classification diagram discriminating sediments according to logarithmic ratios of $SiO_2/Al_2O_3Fe_2O_3/K_2O$ after (Herron, 1988) and **(c)** Quartz crystalline provenance of Nari sandstone after (Crook, 1974), K_2O wt.% versus Na_2O wt.% bivariate diagram.

an average of 30.80 wt. % respectively and these values indicate low weathering conditions during the deposition of Nari sediments (Fig. 5a-c).

Paleo-climatic conditions. According to (Suttner and Dutta, 1986) he proposed a binary SiO_2 wt. % versus ($Al_2O_3 + K_2O + NaO_2$) wt. % diagram to constrain the climatic condition during sedimentation of silica clastic sedimentary rocks. The diagram presented by (Suttner and Dutta, 1986) is used here for sandstone of Nari formation in order to classify the maturity of sandstone as a function of climate. The samples were plotted and revealed less chemical maturity and arid conditions for sandstone of Nari formation (Fig. 6).

SiO_2/Al_2O_3 ratios are sensitive to sediment recycling and weathering and can be used as a sediment maturity indicator and quartz survives preferentially to feldspars, mafic minerals and lithics with increasing sediment maturity (Roser *et al*., 1996; Roser and Korsch, 1986). Average SiO_2/Al_2O_3 ratios in unaltered igneous rocks range from ~3.0 (basic rocks) to ~5.0 (acidic rocks). Values of SiO_2/Al_2O_3 ratio > 5.0 in sandstones are an indication of progressive maturity (Roser *et al*., 1996).

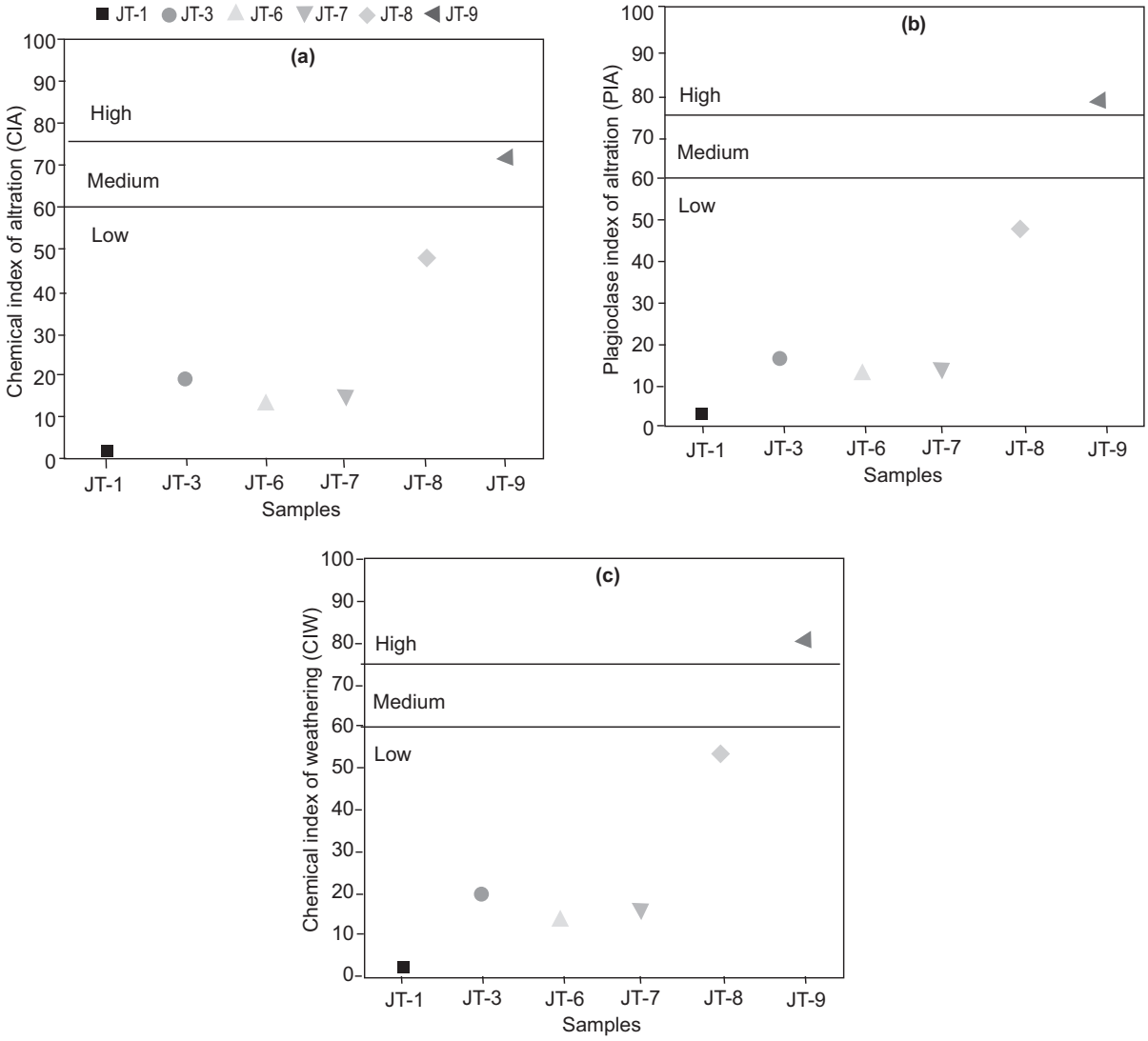

Fig. 5. **(a)** Chemical index of alteration (CIA) is calculated by formula is CIA = {Al_2O_3 / (Al_2O_3 + CaO + NaO_2 + K_2O)} × 100, **(b)** Plagioclase index of alteration (PIA) is calculated by PIA = [(Al_2O_3- K_2O)/(Al_2O_3+ CaO* +NaO_2 - K_2O)] ×100) and **(c)** Chemical index of weathering (CIW) is calculated by CIW = {Al_2O_3/(Al_2O_3 + CaO + NaO_2)} × 100. After (Nesbitt and Young, 1982).

The SiO_2/Al_2O_3 ratios of the sandstones vary from 7.3-9.82 (average ~8.04). Values of K_2O/NaO_2 ratio range from 1.48-4.85 (average ~2.71). Presence of substantial quantities of lithic and feldspar (33 wt. %), low values of SiO_2/Al_2O_3 ratios and high values of K_2O/NaO_2 together point out low to moderate sediment maturity. It is to be noted that the detrital material of sandstones, which has witnessed at least two cycles of chemical weathering at source regions, during transportation and in depocenters still remain poorly to moderately matured. In the present study, sandstone is consist of minor quantities (up to 3 wt. %) of fresh and altered feldspars.

Results and Discussion

Provenance. The provenance of Nari formation sandstone is used to determine by using the discriminant diagram for the provenance of sandstone and mudstone proposed by (Roser and Korsch, 1988). The diagram is divided into four fields, Felsic igneous provenance, Intermediate igneous provenance, Quartzose sedimentary provenance and Mafic igneous provenance. The sandstone samples of Nari formation are plotted mostly in the intermediate to Mafic igneous provenance (Fig. 7).

Tectonic setting. Numerous researches have also shown that chemical compositions of silici-clastic sandstones are significantly governed by plate tectonic settings of their provenance and depositional basins, resulting in the possession of terrain specific geochemical signature of silici-clastic rocks from different tectonic settings (Hakro *et al*., 2021; Bhatia and Crook, 1986; Roser and Korsch, 1986; Bhatia, 1983). Tectonic setting of sandstone from Nari formation is determined by using the different diagrams of tectonic setting on the basis of major oxides concentration. The discriminant diagram by (Roser and Korsch, 1986) is used for plotting the value of SiO_2 wt.% along the X-axis and log (K_2O/NaO_2) along the Y-axis. The diagram is divided into three fields, Passive margin (PM), Active continental margin (ACM) is an Island Arc (IA). All samples of sandstone from Nari formation are plotted into the Active Continental Margin (ACM) (Fig. 8a).

Tectonic discriminant diagram of (Roser and Korsch, 1986) is used for plotting the SiO_2 in (wt. %) along the X-axis versus K_2O/NaO_2 ratio along the Y-axis. The diagram is used to differentiate between three fields, Passive margin (PM), Active continental margin (ACM) and Oceanic island arc (OIA). Two samples are plotted in the Active continental margin, while two are on the boundary of oceanic Island Arc and remaining two clearly plotted in the oceanic Island Arc (Fig. 8b).

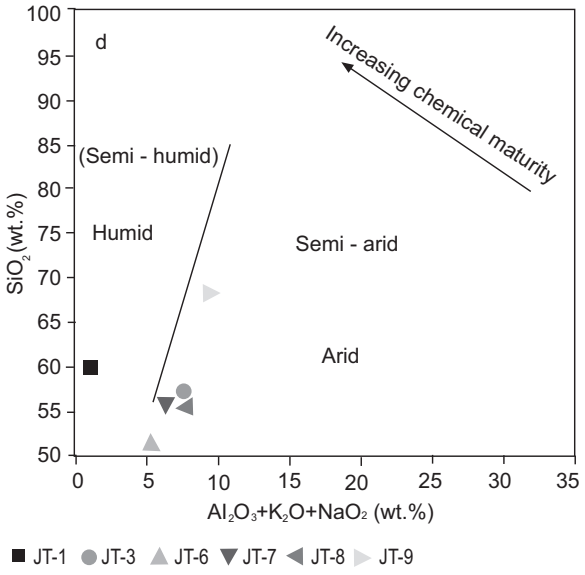

Fig. 6. Chemical maturity of sandstones and their Palaeo-environment of deposition based on SiO_2 wt.% versus ($Al_2O_3 + K_2O + NaO_2$) wt.% bivariate diagram after (Suttner and Dutta, 1986).

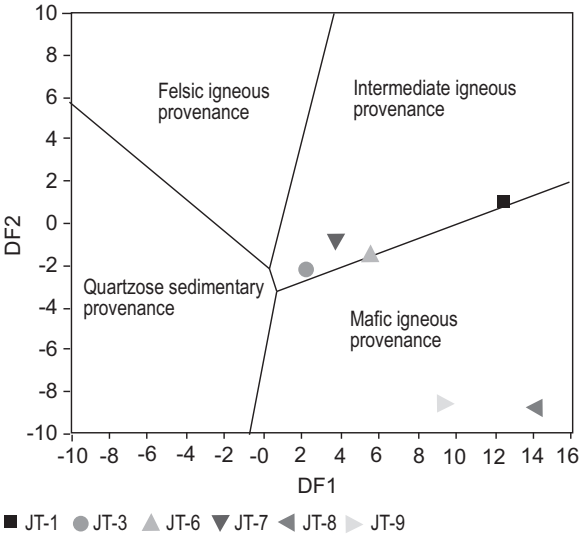

Fig. 7. Provenance and source rock discriminant function : DF1 = -1.773 TiO_2 + 0.607 Al_2O_3 + 0.76 Fe_2O_3T -1.5 MgO + 0.616 CaO + 0.509 NaO_2 -1.224 K_2O -9.09; DF2 = 0.445 TiO_2 + 0.07 Al_2O_3 -0.25 Fe_2O_3 T -1.142 MgO + 0.438 CaO + 1.475 NaO_2 + 1.426 K_2O -6.861diagrams of Nari formation after (Roser and Korsch, 1988).

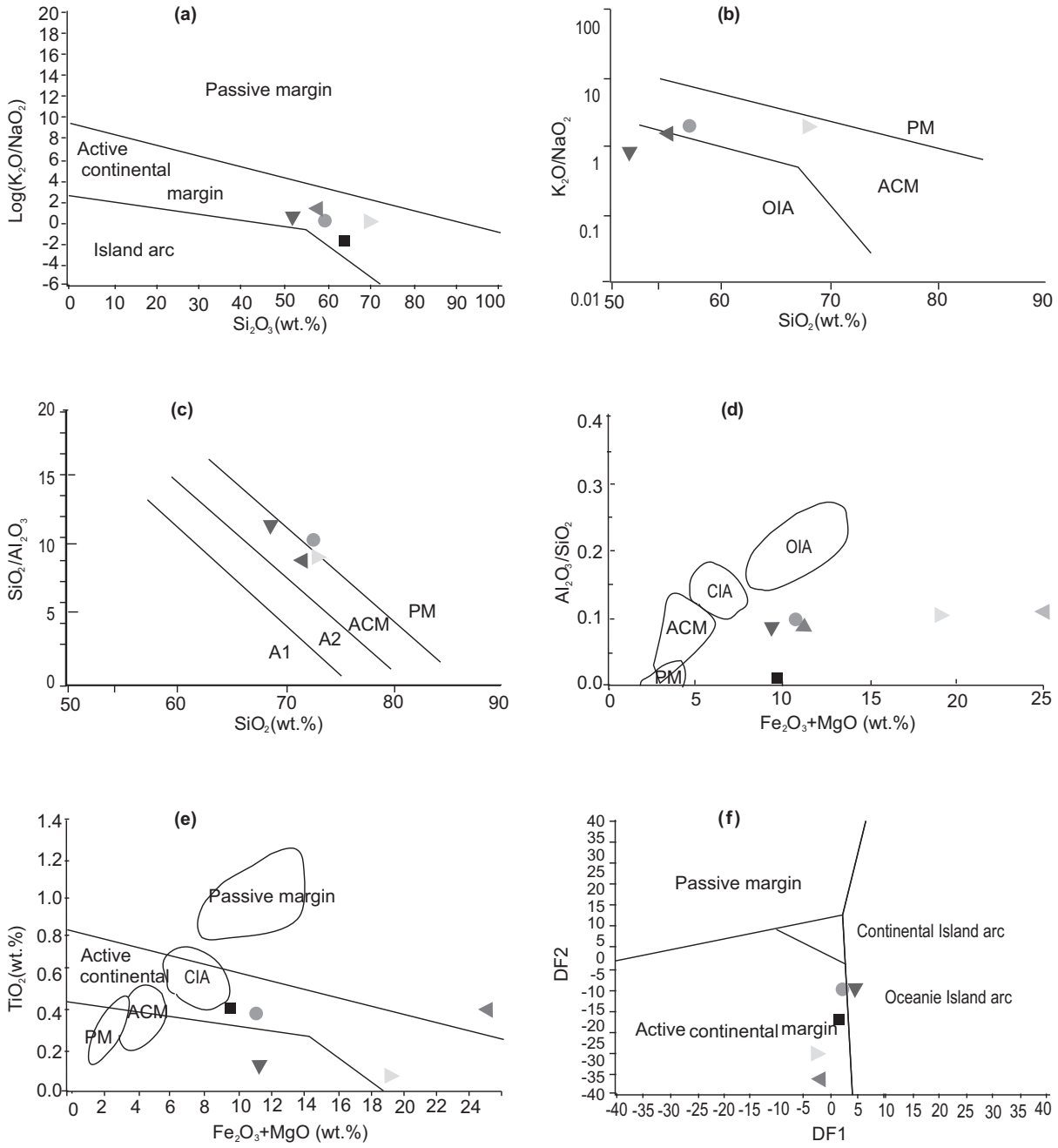

Fig. 8. **(a)** Tectonic setting discrimination diagrams of Nari formation using major elements SiO_2(wt.%) versus log(K_2O/Na_2O) after (Roser and Korsch, 1986), **(b)** Tectonic setting discrimination diagrams of Nari formation SiO_2 (wt.%) versus (K_2O/Na_2O) after (Roser and Korsch, 1986), **(c)** Tectonic discriminant diagram of Nari formation (SiO_2/Al_2O_3 versus K_2O/Na_2O) of (Maynard *et al*., 1982), **(d)** Tectonic setting discrimination diagrams of Nari formation (Al_2O_3/SiO_2 versus Fe_2O_3+MgO) (Bhatia, 1983), **(e)** Tectonic setting discrimination diagrams of Nari formation (TiO_2 in (wt.%) *vs* Fe_2O_3+MgO) (Bhatia, 1983) and **(f)** Tectonic setting discrimination diagrams DF1 = -0.0447 SiO_2 -0.972 TiO_2 + 0.008 Al_2O_3 -0.267 Fe_2O_2T + 0.208 FeO -3.08 MnO + 0.140 MgO + 0.195CaO + 0.719 NaO_2 -0.032 K_2O + 7.510 P_2O_5 + 0.303; DF2 = -0.421 SiO_2 + 1.988 TiO_2 - 0.526 Al_2O_3 -0.551 Fe_2O_3 T -1.610 FeO + 2.720 MnO + 0.881 MgO - 0.907 CaO - 0.177 NaO_2 -1.840 K_2O + 7.244 P_2O_5 + 43.57 of the Nari formation after (Bhatia, 1983).

Tectonic discriminate diagram of (Maynard *et al*., 1982) is used by plotting the ratios of SiO_2/Al_2O_3 along the Y-axis versus K_2O/NaO_2 along the X-axis. The diagram is divided into four fields such as arc setting, basaltic and Andesitic detritus (A1), evolved arc setting, Felsic-plutonic detritus (A2), Active Continental Margin (ACM) and Passive Margin (PM). The majority of the samples are plotted in the active continental margin (Fig. 8c).

Tectonic discriminate diagram of (Bhatia, 1983) is used by plotting the Al_2O_3/SiO_2 ratios along the Y-axis and Fe_2O_3+MgO in wt. % along the X-axis. The diagram is divided into four fields such as passive margin (PM), Active Continental Margin (ACM), Continental Island Arc (CIA) and Oceanic Island Arc (OIA). Five samples out of six are plotted in the sequence of Active Continental Margin (ACM) (Fig. 8d).

Tectonic discriminate diagram of (Bhatia, 1983) is used by plotting the TiO_2 (wt. %) along the Y-axis and Fe_2O_3+MgO along the X-axis. The diagram is divided into four fields such as Passive Margin (PM), Active Continental Margin (ACM), Continental Island Arc (CIA) and Oceanic Island Arc (OIA). Four samples out of six are plotted along the sequence of Active Continental Margin (ACM) and Continental Island Arc (CIA), whereas the two samples are plotted along the Passive Margin (PM) (Fig. 8e).

Another diagram is used for tectonic setting of Nari sandstone to confirmed the tectonic history named (Bhatia, 1983). The diagram is divided into three fields Passive Margin (PM), Oceanic Island Aarc (OIA), Continental Island Arc (CIA), Active Continental Margin (ACM). All the samples of Nari sandstone are plotted in the Active Continental Margin (ACM) and on the boundary line of oceanic island arc (Fig. 8f).

Conclusion

- Geochemical data of studied samples show that these sediments are less mature and composed of some biogenetically and high amount of detrital silica and transported as detrital particles and deposited under the fluvial-deltaic depositional system.
- Geochemical classification of Nari sandstone is classified as mostly Subarkose, Sub- litharenite, Quartzarenite and as Fe-sand (iron sand), with less weathered in an arid climate.
- Discriminate provenance diagrams indicate the provenance of Nari formation is mafic to the intermediate igneous province and intermediate quartz crystalline provenance.
- The Tectonic setting diagram of Nari formation shows that Nari formation is deposited in an active continental margin.

Acknowledgment

We are thankful to Professor Dr. Imdadullah Siddiqui for his support and providing us a vehicle for the field, Prof. Dr. Muhammad Hassan Agheem for help to analyses samples by XRF and thanks to B.S. students group for the collection of samples while field visit. Mr. Waqar Bhatti, Mr. Maqsood, and Mr. Faique, Centre for Pure and Applied Geology, University of Sindh, Jamshoro, Pakistan.

Conflict of Interest. The authors declare no conflict of interest.

References

Agheem, M.H., Jan, M.Q., Solangi, S.H., Laghari, A., Brohi, I.A., Mastoi, A.S. 2012. Petrography and geochemistry of basalts from Ranikot and Bara nala sections, Laki range, lower Indus basin, Pakistan. *Journal of Himalayan Earth Sciences*, **45:** 3-4.

Bhatia, M.R., Crook, K.A.W. 1986. Trace element characteristics of greywackes and tectonic setting discrimination of sedimentary basins. *Contributions to Mineralogy and Petrology*, **92:** 181-193. https://doi.org/10.1007/BF00375292

Bhatia, M.R. 1983. Plate tectonics and geochemical composition of sandstones. *The Journal of Geology*, **91:** 611-627.

Blanco, G., Abre, P., Ferrizo, H., Gaye, M., Gamazo, P., Ramos, J., Alvareda, E., Saracho, A. 2021. Revealing weathering, diagenetic and provenance evolution using petrography and geochemistry: a case of study from the cretaceous to cenozoic sedimentary record of the SE chaco-paraná basin in Uruguay. *Journal of South American Earth Sciences*, **105:** 102-974.

Crook, K.A.W. 1974. Lithogenesis and geotectonics: the significance of compositional variation in flysch arenites (graywackes).

Dickinson, W.R., Valloni, R. 1980. Plate settings and provenance of sands in modern ocean basins. *Geology*, **8:** 82-86.

Duncan, P.M., Sladen, W.P. 1884. The fossil Echinoidea

from the Khirthar series of nummulitic strata in western Sind. *Mem. Geology Survey India, Palaeontogr Indica*, **14:** l.

Glocker, R., Schreiber, H. 1928. Quantitative Röntgen spectrum analysis by means of cold cathode excitation. *Annals of Physics Journal*, **85:** 1089-1102.

Hakro, A.A.A.D., Samtio, M.S., Mastoi, A.S., Rajper, R.H. 2021. The major elemental composition of middle paleocene sediments of southern Indus basin Pakistan: Implication on provenance. *Earth Science Malaysia (ESMY)*, **5:** 10-18. https://doi.org/10.26480/esmy.01.2021.

Hakro, A.A.A.D., Xiao, W., Yan, Z., Mastoi, A.S. 2018. Provenance and tectonic setting of early Eocene Sohnari member of Laki formation from southern Indus Basin of Pakistan. *Geological Journal*, **53:** 1-17. https://doi.org/10.1002/gj.3011

Hakro, A.A.A.D., Khokhar, Q.D. 2015. Distribution of major elements in sediments of the Bara formation, southern Indus basin, Pakistan. *Sindh University Research Journal*, **47:** 823-828.

Hao, L., Wang, Q., Tao, H., Li, X., Ma, D., Ji, H. 2018. Geochemistry of Oligocene Huagang formation clastic rocks, Xihu Sag, the east China sea shelf Basin: provenance, source weathering, and tectonic setting. *Geological Journal*, **53:** 397-411. https://doi.org/10.1002/gj.2906

Herron, M.M. 1988. Geochemical classification of terrigenous sands and shales from core or log data. *Journal of Sedimentary Research*, **58:** 820-829.

HSC, 1961. *Reconnaissance Geology of Part of West Pakistan*: *A Colombo Plan Co-operative Project*. Government of Canada for the Government of Pakistan.

Iqbal, M.W.A. 1969. Mega-fauna from the Ghazij formation (lower Eocene) Quetta Shahrg area, west Pakistan. Memoirs of the Geological Survey of Pakistan. *Palaeontologia Pakisranica*, **5:** 1-40.

Jacobson, A.D., Blum, J.D. 2003. Relationship between mechanical erosion and atmospheric CO_2 consumption in the New Zealand southern Alps. *Geology*, **31:** 865-868.

Kassi, A.M., Kelling, G., Kasi, A.K., Umar, M., Khan, A.S. 2009. Contrasting late Cretaceous-Palaeocene litho stratigraphic successions across the Bibai Thrust, western Sulaiman fold-thrust belt, Pakistan: their significance in deciphering the early collisional history of the NW Indian Plate margin. *Journal of Asian Earth Sciences*, **35:** 435-444. https://doi.org/10.1016/j.jseaes.2009.02.006

Kettanah, Y.A., Armstrong-Altrin, J.S., Mohammad, F.A. 2021. Petrography and geochemistry of siliciclastic rocks of the middle Eocene Gercus formation, northern Iraq: implications for provenance and tectonic setting. *Geological Journal*, **56:** 2528-2549.

Khan, M.H. 1968. The dating and correlation of the Nari and Gaj formations. *Geological Bulletin of Punjab University (Lahore)*, **7:** 57-65.

Khokhar, Q.D., Solangi, S.H., SIddiqui, I., Hakro Daahar, A.A.A. 2016. Sedimentological characterization of Bara formation sandstone, Bhit Nala section, Laki range southern Indus Basin, Pakistna. *Sindh University Research Journal*, **48:** 883-890.

Li, J., Zhang, X., Tian, J., Liang, Q., Cao, T. 2021. Effects of deposition and diagenesis on sandstone reservoir quality: a case study of Permian sandstones formed in a braided river sedimentary system, northern Ordos basin, northern China. *Journal of Asian Earth Sciences*, **213:** 104745.

Mahmud, S.A., Sheikh, S.A. 2009. Reservoir potential of lower Nari sandstones (Early Oligocene) in southern Indus basin and Indus offshore. In: *Annual Technical Conference (ATC)*, pp. 7-8.

Maravelis, A.G., Offler, R., Pantopoulos, G., Collins, W.J. 2021. Provenance and tectonic setting of the early Permian sedimentary succession in the southern edge of the Sydney Basin, eastern Australia. *Geological Journal*, **56:** 2258-2276.

Maynard, J.B., Valloni, R., Yu, H.-S. 1982. Composition of modern deep-sea sands from Arc-related basins. Geological Society, London. *Special Publications*, **10:** 551-561.

Nasir, K, Ahmed, A.K., Peimin, Z. 2013. Integrated geophysical study of the lower Indus platform basin area of Pakistan. *International Journal of Geosciences*, **4:** 9. DOI:10.4236/ijg.2013.49126

Nesbitt, H.W., Young, G.M. 1996. Petrogenesis of sediments in the absence of chemical weathering: effects of abrasion and sorting on bulk composition and mineralogy. *Sedimentology*, **43:** 341-358.

Nesbitt, H.W., Young, G.M. 1982. Early proterozoic climates and plate motions inferred from major element chemistry of lutites. *Nature*, **299:** 715-717. https://doi.org/10.1038/299715a0

Pettijohn, F.J., Potter, P.E., Siever, R. 1972. Introduction and source materials. In: *Sand and Sandstone. Springer*, pp. 1-23.

Roser, B.P., Cooper, R.A., Nathan, S., Tulloch, A.J.

1996. Reconnaissance sandstone geochemistry, provenance, and tectonic setting of the lower Paleozoic terranes of the west Coast and Nelson, New Zealand. *New Zealand Journal of Geology and Geophysics*, **39:** 1-16.

Roser, B.P., Korsch, R.J. 1988. Provenance signatures of sandstone-mudstone suites determined using discriminant function analysis of major element data. *Chemical Geology*, **67:** 119-139. https://doi.org/10.1016/0009-2541(88)90010-1

Roser, B.P., Korsch, R.J. 1986. Determination of tectonic setting of sandstone mudstone suites using content and ratio. *The Journal of Geology*, **94:** 635-650.

Samtio, M., Hakro, A.A.A., Lashari, R., Mastoi, A.S., Rajper, R., Agheem, M. 2021. Depositional environment of Nari formation from Lal Bagh section of Sehwan area, Sindh Pakistan. *Sindh University Research Journal, (Science Series)*, **53:** 67-75.

Shah, S.M.I. 2009. Stratigraphy of Pakistan. Government of Pakistan. Ministry of Petroleum and Natural Resources, *Geological Survey of Pakistan, Memoirs of the Geological Survey of Pakistan*.

Shar, A.M. 2021. Petrography and geochemical characteristics of Nari sandstone in lower Indus basin, Sindh, Pakistan. *Mehran University Research Journal of Engineering and Technology*, **40:** 82-92. https://doi.org/10.22581/muet1982.2101.08

Suttner, L.J., Dutta, P.K. 1986. Alluvial sandstone composition and paleoclimate, I, Framework mineralogy. *Journal of Sedimentary Research*, **56:** 329-345.

Taylor, S.R., McLennan, S.M. 1985. *The Continental Crust: its Composition and Evolution*, 312 pp., Blackwell, Oxford, UK.

Yan, Y., Xia, B., Lin, G., Cui, X., Hu, X., Yan, P., Zhang, F. 2007. Geochemistry of the sedimentary rocks from the Nanxiong basin, south China and implications for provenance, paleo-environment and paleoclimate at the K/T boundary. *Sedimentary Geology*, **197:** 127-140.